



HAL
open science

SUGT1 controls susceptibility to HIV-1 infection by stabilizing microtubule plus-ends

Awatef Allouch, Cristina Di Primio, Audrey Paoletti, Gabrielle Lê-Bury, Frédéric Subra, Valentina Quercioli, Roberta Nardacci, Annie David, Héra Saidi, Anna Cereseto, et al.

► **To cite this version:**

Awatef Allouch, Cristina Di Primio, Audrey Paoletti, Gabrielle Lê-Bury, Frédéric Subra, et al.. SUGT1 controls susceptibility to HIV-1 infection by stabilizing microtubule plus-ends. *Cell Death and Differentiation*, 2020, Online ahead of print, pp.18 - 22. 10.1038/s41418-020-0573-5 . pasteur-02868173

HAL Id: pasteur-02868173

<https://pasteur.hal.science/pasteur-02868173>

Submitted on 18 Jun 2020

HAL is a multi-disciplinary open access archive for the deposit and dissemination of scientific research documents, whether they are published or not. The documents may come from teaching and research institutions in France or abroad, or from public or private research centers.

L'archive ouverte pluridisciplinaire **HAL**, est destinée au dépôt et à la diffusion de documents scientifiques de niveau recherche, publiés ou non, émanant des établissements d'enseignement et de recherche français ou étrangers, des laboratoires publics ou privés.

SUGT1 controls susceptibility to HIV-1 infection by stabilizing microtubule plus-ends

Awatef Allouch¹⁻⁴, Cristina Di Primio⁵, Audrey Paoletti¹⁻⁴, Gabrielle Lê-Bury⁶⁻⁸, Frédéric Subra⁹, Valentina Quercioli⁵, Roberta Nardacci¹⁰, Annie David¹¹, Hela Saidi¹², Anna Cereseto¹³, David M. Ojcius^{14,15}, Guillaume Montagnac¹⁶, Florence Niedergang⁶⁻⁸, Gianfranco Pancino¹¹, Asier Saez-Cirion¹¹, Mauro Piacentini^{10,17}, Marie-Lise Gougeon¹², Guido Kroemer^{8,18-22} and Jean-Luc Perfettini^{1-4,14}

¹ Cell death and Aging team, Gustave Roussy Cancer Campus, F-94805 Villejuif, France;

² Laboratory of Molecular Radiotherapy, INSERM U1030, Gustave Roussy Cancer Campus, F-94805 Villejuif, France;

³ Gustave Roussy Cancer Campus, F-94805 Villejuif, France;

⁴ Université Paris Sud Saclay, 114 rue Edouard Vaillant, F-94805 Villejuif, France;

⁵ Bio@SNS Laboratory, Scuola Normale Superiore, Piazza dei Cavalieri 7, 56126 Pisa, Italy;

⁶ INSERM U1016, Institut Cochin, F- 75013 Paris, France;

⁷ CNRS, UMR 8104, F- 75013 Paris, France;

⁸ Université Paris Descartes, Université de Paris, F-75006 Paris, France;

⁹ CNRS UMR 8113 LBPA, Ecole Normale Supérieure de Cachan, 61 avenue du Président Wilson, F-94230 Cachan, France;

¹⁰ National Institute for Infectious Diseases "Lazzaro Spallanzani", Via Portuense 292, I-00149 Rome, Italy;

¹¹ Unité HIV inflammation and Persistence, 28 rue du Dr Roux, F-75015 Paris, France;

¹² Antiviral Immunity, Biotherapy and Vaccine Unit, Institut Pasteur 25 rue du Dr. Roux, F-75015 Paris, France;

¹³ Laboratory of Molecular Virology, University of Trento, Centre for Integrative Biology, Via Sommarive 9, I-38123 Povo (Trento), Italy;

¹⁴ Department of Biomedical Sciences, University of the Pacific, Arthur Dugoni School of Dentistry, San Francisco, CA 94103;

¹⁵ Université de Paris, F-75013 Paris France;

¹⁶ INSERM U1170, Gustave Roussy Cancer Campus, F-94805 Villejuif, France;

¹⁷ Department of Biology, University of Rome "Tor Vergata", Via della Ricerca Scientifica 1, I-00173, Rome, Italy;

¹⁸ INSERM U848, Gustave Roussy Cancer Campus, F-94805 Villejuif, France;

¹⁹ Metabolomics Platform, Gustave Roussy Cancer Campus, F-94805 Villejuif, France;

²⁰ Equipe 11 labellisée Ligue contre le Cancer, Centre de Recherche des Cordeliers, INSERM U1138, F-75006 Paris, France;

²¹ Pôle de Biologie, Hôpital Européen Georges Pompidou, AP-HP, F-75015 Paris, France;

²² Karolinska Institute, Department of Women's and Children's Health, Karolinska University Hospital, S-17176 Stockholm, Sweden.

The authors declare they have no conflicts of interest

Running title: SUGT1 stabilizes microtubules for HIV-1 infection

Keywords: HIV-1; microtubules; nuclear import; SUGT1

Corresponding author:

Dr. Jean-Luc PERFETTINI
Cell death and Aging team
Laboratory of Molecular Radiotherapy, INSERM U1030
Gustave Roussy Cancer Campus
F-94805 Villejuif, France
Tel. 33-1-42 11 54 24
Fax 33-1-42 11 66 65
e-mail: perfettini@orange.fr
ORCIDid: <https://orcid.org/0000-0002-2427-2604>

54 **Abstract**

55 Understanding the viral-host cell interface during HIV-1 infection is a prerequisite for the
56 development of innovative antiviral therapies. Here we show that the suppressor of G2 allele
57 of *skp1* (SUGT1) is a permissive factor for human immunodeficiency virus (HIV)-1 infection.
58 Expression of SUGT1 increases in infected cells on human brain sections and in permissive
59 host cells. We found that SUGT1 determines the permissiveness to infection of lymphocytes
60 and macrophages by modulating the nuclear import of the viral genome. More importantly,
61 SUGT1 stabilizes the microtubule plus-ends (+MTs) of host cells (through the modulation of
62 microtubule acetylation and the formation of end-binding protein 1 (EB1) comets). This effect
63 on microtubules favors HIV-1 retrograde trafficking and replication. SUGT1 depletion
64 impairs the replication of HIV-1 patient primary isolates and mutant virus that is resistant to
65 raltegravir antiretroviral agent. Altogether our results identify SUGT1 as a cellular factor
66 involved in the post-entry steps of HIV-1 infection that may be targeted for new therapeutic
67 approaches.

68

69

70

71

72

73

74

75

76

77 **Introduction**

78 The design of novel therapeutic antiviral approaches to inhibit the replication of drug-resistant
79 HIV-1 strains assumes a detailed understanding of the cellular factors that promote viral
80 replication steps. Independently from the process of viral entry into target cells, HIV-1 rapidly
81 traffics on stable microtubules, which are characterized by high acetylation levels of α -tubulin
82 at lysine 40 (K40), to reach the nucleus and integrate in the human genome (1, 2). A large list
83 of microtubule-binding proteins is involved in HIV-1 uncoating and stabilization of viral
84 complexes to accomplish reverse transcription and cytoplasmic viral trafficking (reviewed in
85 (3)). Since the suppressor of G2 allele of *S phase kinase associated protein-1 (skp1)* (SUGT1)
86 protein can attach proteins onto microtubules (4-8), we investigated the role of SUGT1 in the
87 early cellular response to HIV-1 infection. Initially described as a co-chaperone of heat shock
88 protein 90, SUGT1 is involved in the innate immune response in plants and mammals (9)
89 through the activation of nucleotide binding domain and leucine-rich repeat containing
90 (NLRP) proteins. Here, we showed that SUGT1 is a permissive cellular factor for HIV-1
91 infection. We demonstrated that SUGT1 promotes HIV-1 reverse transcription and nuclear
92 import through the stabilization of microtubule plus-ends that are required for efficient HIV-1
93 cytoplasmic trafficking. Altogether, our results identify and characterize SUGT1 as a cellular
94 factor that is essential for early steps of HIV-1 infection.

95

96 **Materials and Methods**

97

98 **Cells and reagents**

99 Buffy coats from healthy donors were obtained through the French blood bank (Etablissement
100 Français du sang (EFS)) as part of EFS-INSERM Convention in accordance with French law.
101 Monocytes were obtained from buffy coats and differentiated into macrophages as previously
102 described (10). Monocytes were first separated from peripheral blood mononuclear cells
103 (PBMCs) by adherence to the plastic and then cultured for 6 to 7 days in hydrophobic Teflon
104 dishes (Lumox; Duthsher) in macrophages medium (RPMI 1640 supplemented with 200 mM
105 L-glutamine, 100 U of penicillin, 100 µg streptomycin, 10 mM HEPES, 10 mM sodium
106 pyruvate, 50 µM β-mercaptoethanol, 1% minimum essential medium vitamins, 1% non-
107 essential amino acids) containing 15% of heat inactivated human serum AB. MDMs were
108 then harvested and suspended in macrophage medium containing 10% of heat inactivated
109 fetal bovine serum (FBS). Flow cytometry analysis using anti-CD14 (eBioscience, #12-0149-
110 42), anti-CD11b (Pharmingen, #557918), anti-CD71 (Pharmingen, #555537), anti-CD163
111 (Pharmingen, #562669), anti-CD206 (Pharmingen, #551135) antibodies revealed that 91 to 96
112 % of MDMs expressed both differentiation (CD14, CD11b and CD71) and M2 macrophage
113 (CD163 and CD206) markers. The purity of MDMs was also controlled by the negative
114 staining for anti-CD56 (#560916) (NK cells), anti-CD3 (#555339) (T cells) and anti-CD20
115 (#559776) (B cells) antibodies. All antibodies used were from Pharmingen. The PBLs were
116 isolated from the non-adherent PBMCs fraction using T cells negative selection kit (STEM
117 CELL). Lymphocytes obtained by this method were 90 to 97% CD3 expressing T cells and
118 were cultured in RPMI medium containing 10% FBS. T lymphocytes (5×10^6 /ml) were
119 stimulated by phytohemagglutinin (PHA-P) (5 µg/ml) for 72 hours in medium containing IL-
120 2 (25 units/ml) (Roche), suspended at 10^6 /ml in IL2 medium and cultured for additional two

121 days for Western blot (WB) analysis of SUGT1 expression level and HIV-1 infection, and
122 three days for SUGT1 mediated siRNA silencing. Activation of T cells was determined with
123 anti-CD25 (BD Pharmigen, #560987) and anti-CD69 (BD Pharmigen, #557049) antibodies
124 by flow cytometry. HeLa CD4⁺CXCR4⁺, HEK293T cells and U2OS cell lines were obtained
125 from Prof. Guido Kroemer (Gustave Roussy Cancer Campus, France) and HeLa cells were
126 obtained from Dr. Guillaume Montagnac (Gustave Roussy Cancer Campus, France). These
127 cell lines were cultured in Dulbecco's modified Eagle's medium (DMEM)-Glutamax
128 supplemented with 10% FBS and 100 UI/ml penicillin-streptomycin. All cell lines used were
129 mycoplasma-free.

130

131 **Human autopsies**

132 Human autopsies from frontal cortex were obtained in accordance with Italian and EU
133 legislations, after approval by the Institutional Review Board of the Italian Lazzaro
134 Spallanzani National Institute for Infectious Disease (Ethics Committee approval number
135 40/2006). Post-mortem frontal cortex sections were obtained from three uninfected
136 individuals and nine individuals with HIV-1-associated dementia (all men, mean age 36
137 years; the median values of HIV-1 viral load was $4.5 \pm 0.6 \log_{10}$ cp/ml and < 500 CD4 T
138 cells/ml). All individuals consented to the research use of their frontal cortex brain autopsies
139 at post-mortem.

140

141 **RNA interference**

142 The siGenome smart small interfering RNAs (siRNAs) were all purchased from Dharmacon.
143 The siRNA against SUGT1 (siSUGT1) gene is composed a pool of four siRNAs. The
144 indicated siRNAs have the following sequences: siSUGT1: (1) 5'-
145 GAUCAAGAAUGUUCAGAAG-3', (2) 5'-GAACUUCUUCAUCCUAUAA-3', (3) 5'-

146 GCAAAGAAGUCUCUAGAAC-3' and (4) 5'- GAACCUAUAUCCAUCAUCA-3'. The
147 control siRNA is a pool of four on target plus non-targeting siRNAs (siCo.). The single
148 siRNA against SUGT1 (siSUGT1-1) used for HeLa CD4⁺CXCR4⁺ cell lines was previously
149 described (9): 5'AAGGCUUUGGAACAGAAACCA-3' and the corresponding control
150 siRNA: 5'-UUCAAUAAAUUCUUGAGGU-3' were both synthesized from Sigma.
151 Macrophage silencing was previously described with some modifications (10). Briefly,
152 MDMs (1x10⁶/ml of macrophages medium + 10% FBS) were allowed to be attached at 37°C
153 for 2 hours prior to siRNAs transfection, which was performed with the INTERFERin
154 (Polyplus Transfection). siSUGT1 or siCo. (8 µl from 20 µM stock solution) were pre-diluted
155 in 1 ml of Opti-MEM in which 40 µl of INTERFERin were added and the transfection mix
156 was incubated at room temperature for 10 minutes. The transfection mix (500 µl) was added
157 to 10⁶ for 50 nM final siRNA concentration. MDMs were then incubated at 37°C for 24 hours
158 and the medium was replaced with fresh macrophage medium supplemented with 10% FBS
159 for additional 48 hours prior infections. Activated lymphocytes were suspended in RPMI-IL2
160 medium (10⁷ PBLs/ml) to which 125 µl of the transfection mix containing: 1 ml Opti-MEM,
161 20 µl INTERFERin and 4 µl of siRNA from 20 µM stock solution were added for 6.25 nM
162 final siRNA concentration. After six hours incubation, PBLs were suspended in fresh RPMI-IL2
163 medium (5 10⁶ cells/ml) and cultured for additional 72 hours prior HIV-1 infection. For
164 HeLa, HEK293T and U2OS cells, the final siRNAs concentrations were at 10 picomol
165 transfected with RNAi MAX (Promega) following the manufacturer's instructions. Cell
166 lysates were assayed for protein expression by Western blot to determine the knockdown
167 efficiency at infection at 72 hours for MDMs, PBLs and HEK293T cells and 48 hours for
168 U2OS and HeLa cells post-silencing. Cell viability and cytotoxicity following silencing were
169 determined by WST-1 assay, MTT assay or the lactate dehydrogenase (LDH) release assay
170 (all from Sigma).

171

172 **Plasmid transfections**

173 HEK293T cells (2.5×10^6) were transfected with 5 μ g pcDNA3-HA-IN (HA-IN) pcDNA3-HA
174 (HA) empty vector using Fugene (Promega). After 48 hours of transfection, cells were
175 harvested for co-immunoprecipitation assays. U2OS cells (5×10^3) were silenced by siSUGT1
176 (20 nM) and siControl siRNAs using RNAi max (Qiagen) and at 24 hours later were
177 transfected with 0.5 μ g pcDNA3-HA-IN or pcDNA3-HA for 24 hours. For bulk SUGT1
178 overexpression, HEK293T cells (10^5) were transfected with 0.75 μ g of pCMV-SPORT6-
179 SUGT1 (SUGT1) or pEGFP-N1-GFP control plasmid using Fugene (Promega). After 48
180 hours of transfection, cells were infected and analysed by western blots. For GFP-based flow
181 cytometry sorting, HEK293T cells (10^5) were transfected with 0.75 μ g of pRLL-EF1-SUGT1-
182 PGK-GFP using Fugene (Promega). After 48 hours of transfection, the GFP⁻ and GFP⁺ cells
183 were sorted by FACS, kept for further 24 hours prior western blot analysis and infections.

184

185 **Viral constructs, viruses, lentiviral vectors and in vitro infections and transductions**

186 Single round HIV-1 infections were performed with the VSV-G envelop pseudotyped viruses:
187 HIV-1 $_{\Delta\text{EnvNL4-3-Luc}}$ and HIV-1 $_{\Delta\text{EnvNL4-3-IND64E}}$ that contain luciferase as a reporter gene, HIV-
188 1 $_{\Delta\text{EnvNL4-3-GFP-Vpr}}$ that incorporates GFP-Vpr molecules or with HIV-1CMV-GFP-I-SCEI.
189 HIV-1 $_{\Delta\text{EnvNL4-3-Luc}}$, HIV-1 $_{\Delta\text{envNL4-3-IND64E}}$ and HIV-1 $_{\Delta\text{EnvNL4-3-GFP}}$ were obtained through the co-
190 transfection of 3×10^6 HEK293T cells with 20 μ g pNL4.3-Luc Nef- Env-, pD64E, both from
191 NIH AIDS research reagents and 5 μ g pMD2-VSV-G expression vectors following calcium
192 phosphate transfection procedure (Promega). HIV-1 $_{\Delta\text{EnvNL4-3-GFP-Vpr}}$ was obtained through the
193 transfection of 3×10^6 HEK293T cells with 10 μ g pNL4.3-Luc Nef- Env- (NIH AIDS research
194 reagents), 2.5 μ g pGFP-Vpr and 2.5 μ g pMD2-VSV-G expression vectors using Fugene
195 (Promega) following manufacturer's instructions. For HIV-1 $_{\Delta\text{EnvNL4-3-GFP-Vpr}}$ (VSV-G)

196 supernatants harvest at 48 hours post-transfection and were concentrated by 2 hours of
197 ultracentrifugation in 20% (wt/vol) sucrose cushion. VSVG-pseudotyped HIV-1_{CMV-GFP-I-SCEI}
198 was obtained as previously described (11). Briefly, HIV-1_{CMV-GFP-I-SCEI} virions were produced
199 by transient transfection of 3 × 10⁶ HEK293T cells by using 150 nM polyethylenimine (PEI)
200 reagent (Sigma) with 20 µg of pHR-CMVGFP-I-SceI plasmid, 15 µg of pΔ8.91 packaging
201 and 5 µg of pVSV-G envelope expressing plasmid. Supernatants were collected after 48
202 hours, filtered through a 0.45 µm pore size filter and then concentrated by ultracentrifugation
203 in 20% (wt/vol) sucrose cushion. HIV-1_{IN-EGFP} virions (12) were produced by transfecting 3
204 × 10⁶ HEK293T cells by using 150 nM polyethylenimine (PEI) reagent (Sigma) with 6 µg of
205 pVpr-IN-EGFP, 6 µg of pD64E and 1 µg of pVSV-G. Supernatants were collected after 48
206 hours, filtered through a 0.45 µm pore size filter and then concentrated by ultracentrifugation.
207 For replication competent viruses HIV-1_{NL4-3} and HIV-1_{AD8} were obtained through the
208 transfection of 3 × 10⁶ HEK293T cells with 15 µg of pHIV-1-NL4-3 and pHIV-1-AD8
209 following calcium phosphate transfection protocol (Promega). HIV-1_{NL4-3-IN140/148} replication
210 competent virus (13) was pseudotyped with VSV-G to allow its entry in macrophages. Viral
211 particles in the cell supernatant were harvested at 48 hours post transfection, passed through
212 0.45 µm pore size filters and viral titers were determined by p24 content quantification by
213 ELISA (PerkinElmer).

214 MDMs and PBLs (10⁶) were infected with 100 ng p24 of HIV-1_{AD8}, HIV-1_{NL4-3}, HIV-1_{132w},
215 HIV-1_{BXO8}, HIV-1_{DH12} or the VSV-G envelope pseudotyped viruses (HIV-1_{ΔEnvNL4-3-Luc},
216 HIV-1_{ΔEnvNL4-3-IND64E} or HIV-1_{ΔEnvNL4-3-IN140/148}) for four hours at 37°C. For HIV-1 long
217 replication, MDMs or PBLs (10⁶) were infected with 400 ng CAp24 of HIV-1_{AD8} or 200 ng
218 CAp24 HIV-1_{NL4-3}, respectively. Every three days, cell supernatants were harvested and
219 replaced with fresh culture medium (10⁶ MDMs/ml and 2 × 10⁶ PBLs/ml) during 21 days. Viral
220 replication was monitored by quantifying CAp24 release in the cell supernatants using ELISA

221 method (PerkinElmer). For viral cDNA detection with qPCR, the viral stocks were pretreated
222 with benzonase (Sigma) for 20 minutes at room temperature. The infections were determined
223 by p24 content quantification by ELISA (Zeptometrix Crop) in the supernatant of cells, the
224 luciferase activity from HIV-1_{ΔEnvNL4-3-Luc} (VSV-G) in lysed cells using Luciferase kit
225 (Promega) and also by qPCR analysis of HIV-1 cDNA species at different time points. For
226 HIV-1_{CMV-GFP-I-SCEI} (VSV-G) infection, HEK293T cells lines ($0.5 \cdot 10^5$) were transfected with
227 siSUGT1 or siCo siRNAs at 10 picomol in 500 μ l complete medium using RNAi max
228 (Qiagen). At 72 hours post silencing, 1 μ g of pCBASce plasmid encoding ISCEI endonuclease
229 were transfected using Fugene (Promega). Six hours post-transfection cells ($0.2 \cdot 10^6$) were
230 infected using 600 ng p24 of the virus for two hours at 37°C and then fresh medium was
231 replaced and cells were cultured for further 48 hours, detached and let to adhere on poly-L-
232 lysine solution (Sigma) pretreated chamber slides for two hours before fixation in 2% Neutral
233 buffered formalin (Sigma) for 10 minutes. For HIV-1_{ΔEnvNL4-3-GFP-Vpr} (VSV-G) and HIV-1_{IN-}
234 _{EGFP} (VSV-G) infections, U2OS or HeLa cells ($0.2 \cdot 10^5$) were seeded (in a well of 8 wells
235 chamber slides (BD)) and transfected at 10 picomol with siSUGT1 or siCo. siRNAs using
236 RNAi max (Promega). Cells were then infected with 200 ng p24 of HIV-1_{ΔEnvNL4-3-GFP-Vpr}
237 (VSV-G) at 48 hours post-silencing for 4 hours before 2 % neutral buffered formalin (Sigma)
238 fixation for 10 minutes. For HIV-1_{IN-EGFP} (VSV-G) infections, U2OS or HeLa cells at 48
239 hours post- siRNA silencing were infected with 500 ng p24 of the virus with the addition of
240 polybrene (10 μ g/ml) during the different times of infection before fixation with 2 % neutral
241 buffered formalin (Sigma) or with cold methanol for EB1 staining. When U2OS cells were
242 analysed by live imaging microscopy, they were plated in ibidi 8 well chamber slides
243 (ibiTreat) before siRNA transfection.

244 For the lentiviral vectors pLKO.1, pLKO.1-shSUGT1-3'UTR-1
245 (5'CCGGGCTCTCATCGTATTGTGTATACTCGAGTATACACAATACGATGAGAGC

246 TTTT3') and pLKO.1-shSUGT1-3'UTR-2: (5'CCGGATTGTGTATATTCACCTAATGCT
247 CGAGCATTAGGTGAATATACACAATTTTTTG3'), pRLL-EF1-PGK-GFP, PRL-
248 SUGT1-PGK-GFP were produced by transfecting 3×10^6 HEK293T cells with 1 μ g pDM2-
249 VSV-G, 2.5 μ g p Δ 8.91 packaging and 2 μ g the lentiviral vector using JetPRIME transfectant
250 (Polyplus). Supernatants were harvest at 72 hours post-transfection and quantified for p24
251 content by ELISA. MDM (1×10^5) were transduced simultaneously using 1.5 μ g p24 of each
252 pLKO.1-shSUGT1 and/or 2 μ g PRL-
253 SUGT1-PGK-GFP (pSUGT1) and/or with the
254 equal amounts of control empty lentiviral vectors, with the addition of polybrene during
255 transduction (10 μ g/ml), for 6 hours at 37°C and then kept for 72 hours before analysis by
256 WB or infections. HEK293T cells (10^6) were infected with 20 ng CAp24 HIV-1 $_{\Delta$ EnvNL4-3-Luc
257 (VSV-G) after 48 hours of transfection with pCMV-SPORT6-SUGT1 (for SUGT1 bulk
258 transfection) or pEGFP-N1-GFP control plasmid (for SUGT1 bulk transfection) or after 72
259 hours of pRLL-EF1-SUGT1-PGK-GFP transfection and 24 hours after GFP-based flow
260 cytometry sorting.

260

261 **Quantitative PCR**

262 The quantification of the HIV-1 early reverse transcripts (ERT), late Reverse Transcripts
263 (LRTs), 2-LTRs circles and integrated proviruses were performed as previously described
264 (10); (14). DNA was extracted with the DNeasy Tissue Kit (Qiagen) at 6- and 24 hour post-
265 infection (h.p.i.) for ERT detection, 24 and 72 h.p.i. for LRT and 2-LTRs detections, at 48
266 and 72 h.p.i. for integrated proviruses, respectively, in PBLs and MDMs. The qPCR analysis
267 was carried on an ABI prism 7000 Sequence Detection System. The amounts of HIV-1 cDNA
268 copies were normalized to the endogenous reference gene albumin. Standard curve were
269 generated by serial dilutions of a commercial human genomic DNA (Roche).

270

271 **Immunofluorescence, confocal microscopy, SIM and live imaging**

272 Brain autopsies of frontal cortex from three uninfected individuals and three HIV-1 infected
273 persons were obtained in accordance with the Italian and EU legislations, after approval by
274 the Institutional Review Board of the National Institute for Infectious diseases Lazzaro
275 Spallanzani. Autopsies were deparaffinized, rehydrated and subjected to high-temperature
276 antigen retrieval (96°C for 30 minutes) in 10 mM sodium citrate buffer, pH 6. After one hour
277 blocking in 0.1% BSA in PBS, autopsies were incubated at 4°C for overnight with the
278 primary antibodies anti-SUGT1 (Abcam, #ab30931) and anti-CAP24 (Abcam, #ab9044)
279 diluted at 1/20 in 0.1% BSA in PBS. After three washings in PBS, the secondary antibodies
280 anti-rabbit and anti-mouse IgG conjugated to Alexa-fluor 488 (#A11001, #A11034) and 647
281 fluorochromes (#A21245) from Invitrogen, respectively, and/or the recombinant anti-Iba1
282 conjugated to Alexa Fluor 568 with Hoechst 33342 (Invitrogen, #1874027) for nuclei were
283 added at 1/500 dilution for two hours at room temperature. Immunostained autopsies were
284 then mounted onto glass slides with Fluoromount G (Southern Biotech). At least 5 mosaic
285 autopsy fields (115.33x115.33 μm each) were acquired by confocal microscopy (SP8, Leica)
286 using a 63X objective. SP8 confocal microscope is equipped with two PMT and two high
287 sensitivity hybrid detectors. Z series optical sections for autopsies were at 0.8 μm steps.
288 HEK293T, HeLa and U2OS cells were rinsed with PBS, fixed with 2% neutral buffered
289 formalin (Sigma) for 10 minutes, permeabilized for 15 minutes with 0.3% Triton-X100 in
290 PBS, washed twice in PBS and then blocked for one hour at room temperature in 10% FBS in
291 PBS prior to the incubation with the primary antibodies in 10% FBS in PBS for 2 hours at
292 room temperature. For anti-EB1 staining, the fixation was performed with cold methanol on
293 ice for 2 minutes. After three washes in PBS, the secondary antibodies conjugated with
294 Alexa-Fluor 488 (#A11001; #A11034), 546 (#A20189; #A11035) or 647 (#A21245) (1/500,
295 Invitrogen) supplemented with Hoechst 33342 (Invitrogen, #1874027) for nuclei staining in

296 10% FBS in PBS were added to the cells for 30 minutes at room temperature. After three PBS
297 washings, cells were then mounted with Fluoromount G (Southern Biotech), except for SIM
298 visualization U2OS cells were mounted with ProLong antifade mountant (Thermofisher
299 Scientific) and incubated for 5 hours at 30°C prior analysis. The antibodies used for cells
300 immunostaining were: anti-SUGT1 (BD Transduction Laboratories, #61204) for HEK293T
301 cells and PBLs, anti-SUGT1 (Abcam, #ab30931) for U2OS cells, anti-HA (Biolegend,
302 #90513), anti-phospho-H2AX (Ser139) (Millipore,#05-636), anti- α -tubulin (Sigma, #T9026),
303 anti- α -tubulin (Curie Institute, A-R-H#02 2017), anti-acetylated α -tubulin on lysine 40
304 (Sigma, #T6793), anti-EB1 (BD transduction laboratories, #610535), anti-HIV-1-CAp24
305 (Abcam, #ab9044) and anti-Iba1-Alexa-Fluor 568 (Abcam, #ab221003). Cells were mainly
306 imaged by confocal microscopy (SP8, Leica) using hybrid detectors (pinhole airy: 0.6; pixel
307 size: 180 nm) at optimal optical sectioning (OOS) of 0.2 μ m. For acetylated α -tubulin and
308 EB1 comets, the OOS was 0.11 μ m. Fluorescence intensity related to SUGT1 and
309 microtubule expressions were quantified by Image J software in the best focal plan for the
310 total cell expression for at least 100 cells. The number of acetylated α -tubulin signals and the
311 length of EB1 comets at the cell cortex were analyzed on maximum intensity of z projection
312 images obtained by Image J software. Briefly, scan lines were drawn at the levels of cell
313 cortex, EB1 comets. Then, the number of fluorescence intensity peaks for acetylated α -
314 tubulin and the length of EB1 comets were quantified using Image J software. The viral
315 particles of HIV-1 Δ EnvNL4-3-GFP-Vpr (VSV-G) immunofluorescence were performed as
316 previously described (15) and then were visualized by confocal microscopy (SP8, Leica)
317 using hybrid detectors (pinhole airy: 0.6; pixel size: 180 nm) and parameters adjusted for
318 deconvolution by Huygens software (Scientific Volume). For U2OS cells, acquisitions were
319 performed in 3D SIM mode, with a N-SIM structured illumination Nikon microscope before
320 image reconstruction using the NIS Elements software. The system is equipped with an APO

321 TIRF 100x 1.49NA oil immersion, a laser illumination (488nm, 200mW and 561nm,
322 100mW) and an EMCCD DU-897 Andor camera. Images were acquired with the following
323 protocol: a Z stack (0.12 μm step) was acquired. Images were then reconstructed using Nikon
324 elements software. The lateral resolution of SIM microscopy is about 32 nm. The distances
325 between two different fluorochrome-labeled proteins for SIM microscopy images were
326 calculated on one Z-stack and using “Spot function> colocalize spot” functions of Imaris 5.7
327 software (Bitplane AG) on the cropped subcellular area where GFP-labeled HIV-1 particles
328 were detected or not (HIV-1 GFP⁺ or HIV-1-GFP⁻). Briefly, this function determines the mass
329 center of each fluorescent molecule on the raw SIM images and determines the event number
330 of two colocalized molecules in predefined distance segment. Fluorescence from at least 300
331 molecules were quantified and the frequency of the events was determined by dividing the
332 events number in each distance segment by the total event numbers of the analyzed area in the
333 cytoplasm. For U2OS cells, images were also acquired with a high precision wide-field
334 Eclipse NiU Upright Microscope (Nikon) equipped for image deconvolution. Acquisition was
335 performed using a 100 \times Plan Apo VC 1.4 oil objective and a highly sensitive cooled
336 interlined charge-coupled device (CCD) camera (Roper CoolSnap HQ2). Acquired images
337 were denoised using NdSafir software before deconvolution. All microscopy images with
338 saturated signals were excluded. The colocalization threshold Mander’s correlation coefficient
339 and the fluorescence spectrum overlap for colocalization were determined for different
340 fluorochrome-labeled proteins using Image J software, in the cropped subcellular area where
341 GFP-Vpr-labeled HIV-1 was detected in the merged SIM images. The colocalization
342 threshold Mander’s correlation coefficient (with values varying from 0 to 1) is used to
343 quantify the co-localization or the co-occurrence proportion of two fluorescent probes in the
344 same pixels of the region of interest or structure (16). The threshold M1 (tM1) was used to
345 quantify the occurrence of green channel signals (HIV-1_{IN-EGFP}) in the pixels of the detected

346 red channel signals (α -tubulin). For live imaging, U2OS cells depleted for SUGT1 (siSUGT1)
347 and control cells (siCo.) (0.5×10^5) plated in ibidi 8 well chamber slides (ibiTreat) were
348 infected with HIV-1_{IN-EGFP} (VSV-G) (250 ng CAp24) in the presence of polybrene (10 μ g/ml)
349 and Hoechst 33342 (1 μ g/ml) (Invitrogen) and imaged simultaneously at 1 h.p.i. using a
350 confocal spinning disk (CSU-X1M1; Yokogawa) microscope (DMI6000; Leica) equipped
351 with a CoolSnap HQ2 camera (Photometrics) in heating chamber at 37°C with 5% CO₂ for
352 further 3 hours. Three field positions of each condition (siCo or siSUGT1) were imaged
353 using a 63x oil lens (1.4 NA) every 20 min and with at least 40 series of Z stacks. The best
354 focal plan images of the nucleus were then analyzed with Icy software for the mounting of the
355 video and for quantification of infected cells with HIV-1_{IN-EGFP} RTCs/PICs in the nucleus or
356 those with only cytoplasmic viral events.

357

358 **Western blots and immunoprecipitations**

359 Cells were lysed in NEHN lysis buffer (20 mM Hepes pH 7.5, 300 mM NaCl, 0,5% NP40,
360 20% glycerol, 1mM EDTA) provided with protease and phosphatase cocktails inhibitors
361 (Roche). Protein were quantified with Protein assay kit (Biorad) and 30 to 50 μ g of cell
362 extracts were diluted in the Laemmli buffer (Biorad), boiled for 5 min at 95 °C. Proteins were
363 then loaded on the Nupage 10% or 12 % Bis Tris gel (Life Technologies) for electrophoresis
364 separation and blotted on the PVDF (0.45 μ m) transfer membrane (Thermo Scientific). After
365 blocking with 5% bovine serum albumin (BSA), membranes were incubated with the primary
366 antibodies followed by the secondary horseradish peroxidase (HRP) anti-rat and anti-rabbit,
367 anti-mouse antibodies (Southern Biotech, #6180-01; #4050-05 and #1031-05, respectively).
368 For co-immunoprecipitation assays, the Trueblot HRP secondary antibodies used were from
369 eBioscience (#18-8816-33; #18-8817-33). The proteins were revealed by G:Box I CHEMI
370 developer (Syngene, Ozyme) by using Super Signal West pico (Pierce) or ECL prime (GE

371 healthcare). The primary antibodies used were: anti-SUGT1 (BD Transduction Laboratories,
372 #61204), anti-HA (3F10, Roche, #11867423001), anti-GAPDH (Millipore; #MAB374), anti-
373 CAp24 (NIH AIDS research reagents, #4250), anti-Actin (Abcam, #ab49900), anti-acetylated
374 α -tubulin K40 (AcK40- α -tubulin) (Sigma, #T6793), anti- α -tubulin (Sigma, #T9026) and,
375 anti-HIV-1 integrase (IN-2) (Santa-Cruz, #sc-69721) in 5% skimmed milk in TBS-1% tween.
376 For immunoprecipitations, HEK293T cells expressing HA-IN through transfection at 48
377 hours post transfection or U2OS cells infected for 4 hours with HIV-1 $\square_{EnvNL4-3-Luc}$ (VSV-G)
378 were harvest and then lysed in NEHN buffer. Anti-HA (3F10; Roche, #11867423001) or anti-
379 SUGT1 (Abcam, #ab30931) (2.5 μ g) were added to the cell lysates (1 mg) for 12 hours
380 incubation at 4°C on the wheel. Then, 30 μ l of the protein G sepharose 4 fast flow beads (GE
381 healthcare) were added for additional 4 hours incubation. Immuno-complexes immobilized on
382 the beads were washed twice with NEHN buffer (300 mM NaCl) and third time with NEHN
383 buffer (500 mM NaCl), resuspended in Laemmli buffer (Biorad) and boiled at 95°C for 5
384 minutes. Immunocomplexes were then analyzed by WB.

385

386 **Statistical analysis**

387 We used the two-tailed unpaired t-test for two group comparison and the two-way ANOVA
388 test for the multiple comparisons (more than two groups) of the absolute values means, means
389 of frequencies or means of fold changes \pm SEM (standard error of the mean). Fold changes
390 were calculated as the ratio of the mean value from the treated sample to the mean value of
391 the control sample. The statistical tests were represented in the figures for $n > 10$ sample size.
392 When $n < 10$, the experiments were represented as individual data points without error bars.
393 Data were analyzed with Graphpad prism 6 software. Statistical significance was given as * p
394 < 0.05 and ** $p < 0.01$, *** $p < 0.001$, **** $p < 0.0001$.

395

396 **Results**

397 **The SUGT1 protein promotes permissiveness to HIV-1 infection**

398 Confocal immunofluorescence microscopy was used to evaluate SUGT1 expression at the
399 single cell level in brain frontal cortex sections from HIV-1 infected and uninfected persons.
400 Interestingly, infected cells expressed higher levels of SUGT1, as compared to uninfected
401 cells within the same HIV-1 patient brain section or cells in the brain sections of uninfected
402 controls (Fig. 1a-d). These cells also expressed the ionized calcium-binding adaptor protein-1
403 (Iba1, Supplementary Fig. S1a), indicating that SUGT1 is increased in
404 macrophages/microglia of HIV-1 patient brain sections. Furthermore, SUGT1 expression was
405 increased in activated T cells, which are susceptible to HIV-1 infection as compared to resting
406 primary T lymphocytes, which resist HIV-1 infection (Fig. 1e and Supplementary Fig. S1b).
407 The expression of SUGT1 also strongly increased in primary monocyte-derived macrophages
408 (MDMs), which are permissive for HIV-1, compared with monocytes, which are refractory to
409 HIV-1 infection (Fig. 1f and Supplementary Fig. S1c), indicating that SUGT1 expression
410 increases in permissive cells. We then analyzed the impact of SUGT1 depletion on HIV-1
411 replication. SUGT1 was silenced using a smart pool of small interfering RNAs (siSUGT1) in
412 MDMs (Fig. 1g). SUGT1-depleted MDMs were infected with R5-tropic HIV-1_{AD8}, and viral
413 replication was determined by quantifying CAp24 release. SUGT1 depletion strongly
414 suppressed HIV-1 replication without affecting cell viability (Fig. 1j,k and Supplementary
415 Fig. S1d). These results were confirmed in activated primary blood T-lymphocytes (PBLs)
416 (Fig. 1h,m and Supplementary Fig. S1e,f) and in cervical epithelial (HeLa) cells engineered to
417 express CD4/CXCR4 and a Tat-inducible β -galactosidase (β -Gal) (Fig. 1i,n and
418 Supplementary Fig. S1g). These results were corroborated using a different SUGT1 siRNA
419 (siSUGT1-1) (Supplementary Fig. S1h-j) and revealed no effects on CD4 and CXCR4
420 expression levels nor on cell viability (Supplementary Fig. S1k,l). In addition, long term

421 analysis of CAP24 release from MDMs or PBLs that were infected, respectively, with R5-
422 tropic HIV-1_{AD8} or X4-tropic HIV-1_{NL4-3} (Fig. 1o,p and Supplementary Fig. S1m-p) showed
423 that SUGT1 depletion abolished HIV-1 replication and further indicated that SUGT1 is a
424 permissive factor for HIV-1 infection.

425

426 **The early pre-integrative steps of HIV-1 life cycle are controlled by SUGT1**

427 To identify the viral replication steps that are controlled by SUGT1, MDMs and PBLs were
428 silenced for SUGT1 and infected with *luciferase* (Luc)-expressing HIV-1_{ΔEnvNL4-3-Luc} (HIV-
429 1_{VSV-G}), which is defective in the HIV-1 envelope and pseudotyped with a VSV-G envelope
430 (which allows the virus to enter cells by endocytosis). SUGT1 depletion strongly reduced the
431 infectivity of HIV-1_{ΔEnvNL4-3-Luc} (VSV-G) in MDMs (Fig. 2a,b) and PBLs (Fig. 2c,d),
432 implying that SUGT1 modulates post-entry steps. In MDMs (Fig. 2e) and PBLs (Fig. 2f)
433 whose SUGT1 had been depleted by a pool of two short hairpin RNAs (shSUGT1), the
434 expression of SUGT1 cDNA resistant to shSUGT1 restored the infectivity of HIV-1_{ΔEnvNL4-3-}
435 _{Luc} (VSV-G) (Fig. 2g (for MDMs) and Fig. 2h (for PBLs)). Consistently, the exogenous
436 SUGT1 overexpression in HEK293T cells significantly enhanced the infectivity of HEK293T
437 cells with HIV-1_{ΔEnvNL4-3-Luc} (VSV-G) (Supplementary Fig. S2a-d), demonstrating the specific
438 effect of SUGT1 in promoting HIV-1 infection.

439 MDMs and PBLs were then depleted for SUGT1, infected with the same virus and analyzed
440 by quantitative real time PCR (qPCR) for early reverse transcripts (at 24 and 6 hours post-
441 infection (h.p.i.) of MDMs and PBLs, respectively), late reverse transcripts and 2-LTR circles
442 (at 72 and 24 h.p.i, respectively), as well as integrated proviruses (at 72 and 48 h.p.i,
443 respectively). No significant difference in the formation of HIV-1 early reverse transcripts
444 was observed in SUGT1-depleted cells (Fig. 2i,j). A mild decrease of the late reverse
445 transcripts was observed in SUGT1-depleted MDMs (Fig. 2k) or PBLs (Fig. 2l) (as compared

446 with control cells). More importantly, SUGT1 depletion strongly inhibited the formation of 2-
447 LTR circles, a surrogate marker of nuclear viral import, in HIV-1 infected MDMs (Fig. 2m)
448 and PBLs (Fig. 2n). Consequently, the integrated proviruses (detected by the Alu-nested
449 qPCR) were decreased after SUGT1 depletion (Fig. 2o,p). Similar results were obtained when
450 SUGT1-depleted MDMs were infected with R5-tropic HIV-1_{AD8} (Supplementary Fig. S2e-h).
451 The nuclear import (as evaluated by 2-LTR circles qPCR) of a HIV-1 mutant that is defective
452 for integration (HIV-1_{ΔEnvNL4-3-IND64E} (VSV-G)) was also abrogated by the depletion of
453 SUGT1 (Fig. 2q). Considering that mutant HIV-1_{IND64E} translocates efficiently to the nucleus
454 (17), this result implies that SUGT1 regulates HIV-1 pre-integrative phases. To further
455 characterize this process, we infected SUGT1-depleted HEK293T cells with HIV-1_{CMVGFP-I-}
456 _{SCEI} (VSV-G), which encodes GFP as reporter gene and has been engineered by inserting, into
457 the viral DNA, the yeast ISCEI endonuclease cleavage site that is cut when its cognate
458 enzyme is introduced into human cells (11). In this system, the depletion of SUGT1 in
459 HEK293T cells strongly inhibited HIV-1 infection, as revealed by the reduction of the
460 percentage of cells that express immunofluorescent γH2AX-associated foci as well as the
461 expression of virus-encoded GFP (Fig. 2r,s). The lack of GFP detection in SUGT1-depleted
462 cells indicates the absence of 2-LTR's circles forms (which can express the GFP reporter
463 gene) and further suggests that SUGT1 governs the nuclear translocation of HIV-1.
464 Altogether, these data imply that SUGT1 expression dictates HIV-1 permissiveness by
465 promoting HIV-1 reverse transcription and mainly nuclear import.

466

467 **SUGT1 is associated with microtubules bearing HIV-1**

468 Considering the role of SUGT1 in the stabilization and attachment of proteins to the
469 microtubule network (4), we investigated the presence of SUGT1 on microtubules bearing
470 HIV-1. U2OS cells were infected with a VSV-G-pseudotyped HIV-1_{ΔEnvNL4-3}, which

471 incorporates GFP-Vpr (HIV-1_{ΔEnvNL4-3}-GFP-Vpr (VSV-G)) (15), and the subcellular localization
472 of SUGT1, GFP-labeled viral complexes and microtubules was analyzed by super-resolution
473 structured illumination microscopy (SIM) and wide-field high precision microscopy at 4
474 hours post-infection. As expected, at this time point, GFP-labeled viral complexes colocalized
475 with cytoplasmic filaments (Fig. 3aI) and aggregated at microtubule-organizing centers
476 (MTOC) (Supplementary Fig. S3a). Importantly, endogenous SUGT1 molecules were located
477 in close proximity to the microtubule-associated viral complexes (Fig. 3aII). SUGT1, viral
478 complexes, and microtubules often formed ternary structures (Fig. 3aIII-4). Fluorescence
479 overlap spectrum analysis confirmed these results, indicating that the three components
480 (SUGT1, GFP and microtubules) were located within a distance of <0.8 μm (Fig. 3aIII-4). A
481 high colocalization Mander's coefficient (~1) confirmed the tight association of SUGT1 with
482 microtubules that are used by HIV-1 for trafficking in host cells (Supplementary Fig. S3b,c).

483

484 Since HIV-1 integrase (IN) translocates to the nucleus to catalyze the integration of viral
485 cDNA into the human genome, we monitored the subcellular localization of HA-tagged
486 integrase (HA-IN) in SUGT1-depleted U2OS cells. Interestingly, we observed that the
487 silencing of SUGT1 (Fig. 3b) induced a diffused localization of IN in the cytoplasm and the
488 nucleus compared with control cells that had exclusive nuclear localization (Fig. 3c,d),
489 indicating that SUGT1 contributes to the nuclear accumulation of IN. In agreement with a
490 previous report showing that efficient nuclear translocation prevents cytoplasmic degradation
491 of HIV-1 IN (18), protein levels of HA-IN decreased in SUGT1-depleted cells (Fig. 3b).
492 However, no interactions between endogenous SUGT1 and HA-IN were detected by co-
493 immunoprecipitation in HEK293 T cells (Fig. 3e), suggesting that SUGT1 may act on HIV-1
494 nuclear translocation without interacting with viral proteins. Altogether, these data indicate
495 that SUGT1 is associated with microtubules bearing HIV-1.

496

497 **SUGT1 regulates the organization and the stability of the cortical microtubule plus-ends**

498 To understand the mechanism by which SUGT1 contributes to HIV-1 nuclear import, we
499 investigated the effect of SUGT1 on the structural organization of microtubules. Although
500 SUGT1 knockdown did not modify tubulin expression, nor disrupt the global architecture or
501 the density of the microtubule network (Fig. 4a,b and Supplementary Fig. S4a,b), confocal
502 microscopy revealed a significant alteration of the microtubule plus-ends (+MTs)
503 organization at the level of the cell cortex (Fig. 4a,c and Supplementary Fig. S4a). SUGT1-
504 depleted U2OS cells exhibited +MTs that were dissociated and distributed perpendicularly to
505 the cell cortex, while in control cells, the +MTs were clustered and curved in parallel to the
506 cell cortex. Even though the total expression of stable microtubules (AcK40 α -tubulin) was
507 not affected by the SUGT1 knockdown (Supplementary Fig. S4b), the acetylation of +MTs at
508 the cell cortex significantly decreased in U2OS and HeLa cells (Fig. 4d-f and Supplementary
509 Fig. S4c-f). These data indicate that the cortical +MTs, which are the first contact points of
510 HIV-1 with the microtubule network after viral entry, are unstable in SUGT1-depleted cells
511 and thus may not efficiently support the cytoplasmic trafficking of the virus. To confirm this
512 hypothesis, we analyzed whether SUGT1 depletion would affect the organization of the plus-
513 end tracking protein EB1, which promotes the cytoplasmic trafficking of HIV-1 on
514 microtubules (1). Considering that EB1 molecules bind to +MTs and form EB1 comets,
515 whose elongation is associated with an increased growth rate and a decreased stability (19-
516 22), the impact of SUGT1 silencing on the length of EB1 comets was determined. A
517 significant increase in the length of EB1 comets was observed in SUGT1-depleted HeLa and
518 U2OS cells, compared with control cells (Fig. 4g-i and Supplementary Fig. S4g-j), suggesting
519 that in SUGT1-depleted cells, +MTs are less stable and highly dynamic, and thus would not
520 sustain the trafficking of HIV-1 viral particles after viral entry. Taken together, our data

521 reveal that SUGT1 controls the architecture and the stability of +MTs, which are required for
522 the attachment and efficient trafficking of HIV-1 on the microtubule network.

523

524 **SUGT1 is essential for the association of HIV-1 with stable microtubules and its**
525 **translocation to the host cell nucleus**

526 Co-immunoprecipitation assays revealed an interaction between SUGT1 and stable
527 microtubules (Fig. 5a). This interaction was strongly enhanced after 4 hours of infection of
528 U2OS cells with HIV-1 $_{\Delta\text{EnvNL4-3-Luc}}$ (VSV-G), further demonstrating that SUGT1 is associated
529 with the microtubules that are used by HIV-1 for trafficking (Fig. 5a). Using HIV-1 $_{\text{IN-EGFP}}$
530 virus pseudotyped by VSV-G envelope that contains enhanced GFP labeled IN (12, 23), we
531 showed that in SUGT1-depleted U2OS cells, and in contrast to control cells (Fig. 5b), HIV-
532 1 $_{\text{IN-EGFP}^+}$ viral complexes did not aggregate at the MTOC and displayed a diffuse distribution
533 in the cytoplasm (Fig. 5d). Accordingly, the colocalization of HIV-1 $_{\text{IN-EGFP}^+}$ complexes with
534 microtubules significantly decreased in SUGT1-depleted cells (Fig. 5c), suggesting that, in
535 the absence of SUGT1, a defect in the migration to the perinuclear area is associated with a
536 defect in the association of the virus with microtubules. In agreement with the results obtained
537 with HIV-1 IN expressed as a single protein (Fig. 3b), the mean fluorescence intensity of
538 HIV-1 $_{\text{IN-EGFP}^+}$ complexes detected after 4 hours of infection of SUGT1-depleted cells was
539 significantly decreased, as compared with control cells (Supplementary Fig. S5a), indicating
540 that the failed nuclear translocation of HIV-1 induces its rapid cytoplasmic degradation.
541 Moreover, SUGT1 depletion decreased the percentage of cells with HIV-1 $_{\text{IN-EGFP}}$ nuclear
542 events at 4 and 6 h.p.i. and increased the percentage of cells showing only cytoplasmic viral
543 events (Fig. 5e). Consistent with these results, live imaging microscopy showed nuclear
544 translocation of HIV-1 $_{\text{IN-EGFP}^+}$ viral complexes in control U2OS cells (Movie 1), while in the
545 SUGT1-depleted cells, viral complexes did not translocate to the host cell nucleus (Movie 2),

546 leading to a decrease of HIV-1 nuclear events (Supplementary Fig. S5b). Interestingly, a
547 significant elongation of EB1 comets was detected in SUGT1-depleted HeLa cells infected
548 with HIV-1_{IN-EGFP} (VSV-G) (Fig. 5f,g) or HIV-1_{ΔEnvNL4-3-Luc} (VSV-G) (Supplementary Fig.
549 S5c) for 6 hours, as compared with control cells. Accordingly, the nuclear accumulation of
550 HIV-1_{IN-EGFP}⁺ viral complexes was significantly decreased in SUGT1-depleted cells (Fig. 5h).
551 Altogether, these results demonstrate that SUGT1 promotes HIV-1 nuclear import by
552 increasing its association with microtubules and its cytoplasmic trafficking to reach the host
553 nucleus.

554

555 **SUGT1 depletion abolished permissiveness to HIV-1 primary isolates and ART-resistant** 556 **viral mutant**

557 In order to evaluate the potential of SUGT1 inactivation for HIV-1 therapy, we determined
558 the impact of SUGT1 depletion on the permissiveness of MDMs to infection with HIV-1
559 primary isolates (HIV-1_{BX08}, HIV-1_{132W} and HIV-1_{DH12}) and to HIV-1 clone (HIV-1_{140/148}), a
560 double mutant virus that is resistant to raltegravir antiretroviral treatment (ART) (13).
561 Interestingly, SUGT1 depletion strongly inhibited the formation of 2-LTR circles (Fig. 6a-d)
562 and CAp24 release (Fig. 6e-g) from MDMs that were infected with CCR5 (R5) tropic (HIV-
563 1_{BX08} and HIV-1_{132W}) or CCR5/CXCR4 (R5X4) dual tropic (HIV-1_{DH12}) HIV-1 primary
564 isolates (Fig. 6a-e). In addition, the depletion of SUGT1 drastically impaired viral integration
565 (Fig. 6h) and CAp24 release (Fig. 6i) from MDMs that were infected with an HIV-1 double
566 mutant G140S-Q148H in integrase polypeptide (HIV-1_{140/148}) that is resistant to the integrase
567 inhibitor raltegravir. Altogether, these results highlight the potential for SUGT1 as a cellular
568 target to inhibit viral replication and overcome viral resistance to ART.

569

570 **Discussion**

571 In the present study, we demonstrate that SUGT1 is a host factor that determines lymphocyte
572 and macrophage susceptibility to HIV-1 infection and replication via an effect on the post-
573 entry replication steps. SUGT1 stabilizes the +MTs, thereby promoting the association of
574 HIV-1 with stable microtubules, allowing their efficient trafficking to the nuclear pores, and
575 viral import into the nucleus and subsequent integration into the host genome. In contrast to
576 the previously described microtubule-associated proteins (such as EB1 and Kif4 (1-3, 24)),
577 which increase microtubule stability (by enhancing AcK40 α -tubulin) following infection,
578 SUGT1 contributes to maintain the stability of microtubules mainly at the level of the plus-
579 end TIPs, by inhibiting their dynamic and preserving their acetylation. The fact that we
580 showed that SUGT1 expression is upregulated in the HIV-1 permissive activated T cells and
581 macrophages with respect to their cognate resting lymphocytes and monocytes refractory to
582 HIV-1 infection, does not exclude the possible contribution of synergetic pathways involved
583 during differentiation and activation in the stabilization of the microtubules and enhancing the
584 susceptibility to HIV-1. A recent report demonstrated that the rapid proteasome-mediated
585 degradation of the viral cores in the cytoplasm is detected when their uncoating fails to occur
586 progressively up to their trafficking to the nuclear pores (25). Consistent with this report, the
587 intensity of the fluorescent viral complexes, which were mainly accumulated in the cytoplasm
588 of host cells, was significantly decreased in SUGT1-depleted cells, as compared with control
589 cells, suggesting their degradation by proteasomes due to lack of efficient trafficking to the
590 nuclear pores. Similarly, HIV-1 IN was shown to be stabilized on the MTOC, prior to its
591 nuclear translocation, through direct interaction with microtubule-associated proteins (such as
592 the centrosomal protein STU2P (yeast homolog of XMAP215) and the dynein light chain
593 protein DYN2P) (26, 27) and its failure to be recruited to the nucleus leads to its rapid
594 degradation by proteasomes in the cytoplasm of host cells (18). Future studies will explore the

595 potential role of SUGT1 in the trafficking of other viruses that employ the microtubule
596 network, such as Hepatitis C virus, Dengue virus or African Swine Fever virus. Finally, our
597 results demonstrate that SUGT1 should be considered as a target in novel therapeutic
598 strategies to inhibit infection with HIV-1 strains that are resistant to raltegravir antiretroviral
599 treatment (ART).
600

601 **Acknowledgements**

602

603 We acknowledge Dr. Alessandro Donado, Yann Lecluse, Floriane Herit and Pierre
604 Bourdoncle (IMAG³IC facility of Institut Cochin) for their technical support, and Pr. Eric
605 Solary for the pRLL-EF1-PGK-GFP lentiviral vector plasmid. This work was supported by
606 funds from Agence Nationale de la Recherche (ANR-10-IBHU-0001, ANR-10-LABX33 and
607 ANR-11-IDEX-003-01), Cancéropole Ile de France, Electricité de France, Fondation Gustave
608 Roussy, Institut National du Cancer (INCA 9414), NATIXIS, SIDACTION and the French
609 National Agency for Research on AIDS and viral Hepatitis (ANRSH) (to J-L.P. and F.N.).

610

611

612

613 **Conflict of interest**

614

615 The authors declare they have no conflicts of interest.

616

617

618 **References**

619

620 1. Sabo Y, Walsh D, Barry DS, Tinaztepe S, de Los Santos K, Goff SP, et al. HIV-1 induces
621 the formation of stable microtubules to enhance early infection. *Cell Host Microbe*.
622 2013;**14**:535-546.

623

624 2. Delaney MK, Malikov V, Chai Q, Zhao G, Naghavi MH. Distinct functions of diaphanous-
625 related formins regulate HIV-1 uncoating and transport. *Proc Natl Acad Sci U S A*.
626 2017;**114**:E6932-E6941.

627

628 3. Dharan A, Campbell EM. Role of Microtubules and Microtubule-Associated Proteins in
629 HIV-1 Infection. *J Virol*. 2018;**92**:e00085-18.

630

631 4. Andersen RO, Turnbull DW, Johnson EA, Doe CQ. Sgt1 acts via an LKB1/AMPK
632 pathway to establish cortical polarity in larval neuroblasts. *Dev Biol*. 2012;**363**:258-265.

633

634 5. Davies AE, Kaplan KB. Hsp90-Sgt1 and Skp1 target human Mis12 complexes to ensure
635 efficient formation of kinetochore-microtubule binding sites. *J Cell Biol*. 2010;**189**:261-274.

636

637 6. Kitagawa K, Skowyra D, Elledge SJ, Harper JW, Hieter P. SGT1 encodes an essential
638 component of the yeast kinetochore assembly pathway and a novel subunit of the SCF
639 ubiquitin ligase complex. *Mol Cell*. 1999;**4**:21-33.

640

641 7. Liu W, Evanoff DP, Chen X, Luo Y. Urinary bladder epithelium antigen induces CD8+ T
642 cell tolerance, activation, and autoimmune response. *J Immunol*. 2007;**178**:539-546.

643

644 8. Steensgaard P, Garre M, Muradore I, Transidico P, Nigg EA, Kitagawa K, et al. Sgt1 is
645 required for human kinetochore assembly. *EMBO Rep*. 2004;**5**:626-631.

646

647 9. Mayor A, Martinon F, De Smedt T, Petrilli V, Tschopp J. A crucial function of SGT1 and
648 HSP90 in inflammasome activity links mammalian and plant innate immune responses. *Nat*
649 *Immunol*. 2007;**8**:497-503.

650

651 10. Allouch A, David A, Amie SM, Lahouassa H, Chartier L, Margottin-Goguet F, et al. p21-
652 mediated RNR2 repression restricts HIV-1 replication in macrophages by inhibiting dNTP
653 biosynthesis pathway. *Proc Natl Acad Sci U S A*. 2013;**110**:E3997-4006.

654

655 11. Di Primio C, Quercioli V, Allouch A, Gijsbers R, Christ F, Debyser Z, et al. Single-cell
656 imaging of HIV-1 provirus (SCIP). *Proc Natl Acad Sci U S A*. 2013;**110**:5636-5641.

657

658 12. Francis AC, Di Primio C, Quercioli V, Valentini P, Boll A, Girelli G, et al. Second
659 generation imaging of nuclear/cytoplasmic HIV-1 complexes. *AIDS Res Hum Retroviruses*.
660 2014;**30**:717-726.

661

662 13. Delelis O, Malet I, Na L, Tchertanov L, Calvez V, Marcelin AG, et al. The G140S
663 mutation in HIV integrases from raltegravir-resistant patients rescues catalytic defect due to
664 the resistance Q148H mutation. *Nucleic Acids Res*. 2009;**37**:1193-1201.

665

- 666 14. David A, Saez-Cirion A, Versmisse P, Malbec O, Iannascoli B, Herschke F, et al. The
667 engagement of activating FcγR3 inhibits primate lentivirus replication in human
668 macrophages. *J Immunol.* 2006;**177**:6291-6300.
669
- 670 15. McDonald D, Vodicka MA, Lucero G, Svitkina TM, Borisy GG, Emerman M, et al.
671 Visualization of the intracellular behavior of HIV in living cells. *J Cell Biol.* 2002;**159**:441-
672 452.
673
- 674 16. Dunn KW, Kamocka MM, McDonald JH. A practical guide to evaluating colocalization
675 in biological microscopy. *Am J Physiol Cell Physiol.* 2011;**300**:C723-742.
676
- 677 17. Svarovskaia ES, Barr R, Zhang X, Pais GC, Marchand C, Pommier Y, et al. Azido-
678 containing diketo acid derivatives inhibit human immunodeficiency virus type 1 integrase in
679 vivo and influence the frequency of deletions at two-long-terminal-repeat-circle junctions. *J*
680 *Viro.* 2004;**78**:3210-3222.
681
- 682 18. Devroe E, Engelman A, Silver PA. Intracellular transport of human immunodeficiency
683 virus type 1 integrase. *J Cell Sci.* 2003;**116**:4401-4408.
684
- 685 19. Akhmanova A, Steinmetz MO. Control of microtubule organization and dynamics: two
686 ends in the limelight. *Nat Rev Mol Cell Biol.* 2015;**16**:711-726.
687
- 688 20. Bieling P, Kandels-Lewis S, Telley IA, van Dijk J, Janke C, Surrey T. CLIP-170 tracks
689 growing microtubule ends by dynamically recognizing composite EB1/tubulin-binding sites.
690 *J Cell Biol.* 2008;**183**:1223-1233.
691
- 692 21. Matov A, Applegate K, Kumar P, Thoma C, Krek W, Danuser G, et al. Analysis of
693 microtubule dynamic instability using a plus-end growth marker. *Nat Methods.* 2011;**7**:761-
694 768.
695
- 696 22. Seetapun D, Castle BT, McIntyre AJ, Tran PT, Odde DJ. Estimating the microtubule GTP
697 cap size in vivo. *Curr Biol.* 2012;**22**:1681-1687.
698
- 699 23. Albanese A, Arosio D, Terreni M, Cereseto A. HIV-1 pre-integration complexes
700 selectively target decondensed chromatin in the nuclear periphery. *PLoS One.* 2008;**3**:e2413.
701
- 702 24. Fernandez J, Portilho DM, Danckaert A, Munier S, Becker A, Roux P, et al. Microtubule-
703 associated proteins 1 (MAP1) promote human immunodeficiency virus type I (HIV-1)
704 intracytoplasmic routing to the nucleus. *J Biol Chem.* 2015;**290**:4631-4646.
705
- 706 25. Francis AC, Melikyan GB. Single HIV-1 Imaging Reveals Progression of Infection
707 through CA-Dependent Steps of Docking at the Nuclear Pore, Uncoating, and Nuclear
708 Transport. *Cell Host Microbe.* 2018;**23**:536-548 e6.
709
- 710 26. Desfarges S, Salin B, Calmels C, Andreola ML, Parissi V, Fournier M. HIV-1 integrase
711 trafficking in *S. cerevisiae*: a useful model to dissect the microtubule network involvement of
712 viral protein nuclear import. *Yeast.* 2009;**26**:39-54.
713

714 27. de Soultrait VR, Caumont A, Durrens P, Calmels C, Parissi V, Recordon P, et al. HIV-1
715 integrase interacts with yeast microtubule-associated proteins. *Biochim Biophys Acta*.
716 2002;**1575**:40-48.
717

718 **Figure legends**

719

720 **Figure 1. SUGT1 determines HIV-1 permissiveness in human cells.**

721 **(a-c)** Immunofluorescence of brain autopsies from uninfected persons (n=3) **(a)** and HIV-1
722 infected patients (n=3) **(b)** for SUGT1, CAp24 and nucleus. **(c)** Magnification.

723 **(d)** Quantification of SUGT1 expression in CAp24⁺ (n=45) or CAp24⁻ (n=690) cells detected
724 in brain sections. Fluorescence intensities (FI) are shown. Means \pm SEM are indicated. P
725 values were calculated using two-tailed unpaired t-test using Bonferroni correction (*p < 0.1).

726 **(e, f)** Representative human resting/PHA-P/IL2-activated PBLs **(e)** or
727 monocytes/macrophages **(f)** WB of endogenous SUGT1 levels are shown (n=3). SUGT1 a
728 and b isoforms are indicated.

729 **(g-i)** SUGT1 depletion in human MDMs **(g)**, PBLs **(h)** and CD4⁺CXCR4⁺ HeLa cells **(i)** are
730 shown (n=3).

731 **(j-n)** Effect of SUGT1 depletion on viral production obtained from MDMs **(j, k)**, PBLs **(l, m)**
732 or CD4⁺CXCR4⁺ HeLa cells (n=3) **(n)** infected with HIV-1_{AD8} **(j, k)** or HIV-1_{NL4-3} **(l-n)**.
733 CAp24 release for representative donor **(j, l)** and fold changes (n=7 for MDMs, n=3 for
734 PBLs) **(k, m)** are shown.

735 **(o, p)** Effect of SUGT1 depletion on viral production obtained at indicated times post-
736 infection from MDMs **(o)** and PBLs **(p)** infected with HIV-1_{AD8} **(o)** or HIV-1_{NL4-3} **(p)**. CAp24
737 release from representative donors is shown (n=3).

738

739 **Figure 2. SUGT1 promotes early HIV-1 replication steps.**

740 **(a-d)** HIV-1 infectivity of control or SUGT1-depleted MDMs **(a, b)** and activated PBLs **(c, d)**
741 that were infected with HIV-1 _{Δ EnvNL4-3-Luc} (VSV-G) for 72 hours. Luciferase activity from

742 representative donor (**a, c**) and fold changes (n=8 for MDMs and n=4 for PBLs) (**b, d**) are
743 shown.

744 (**e-h**) MDMs (**e**) and PBLs (**f**) were transduced with lentiviral vectors expressing control
745 (shCo.), a pool of two shRNAs against SUGT1 (shSUGT1) and/ or SUGT1 resistant cDNA
746 (pSUGT1) for 72 hours prior infection with HIV-1_{ΔEnvNL4-3-Luc} (VSV-G). WB (**e,f**) and
747 luciferase activity at 48 h.p.i. from representative donors is shown (**g,h**) (n=3).

748 (**i-q**) Fold changes of HIV-1 early reverse transcripts (**i, j**), late reverse transcripts (**k, l**), 2-
749 LTRs circles (**m, n, q**) and integrated proviruses (**o, p**) were determined by qPCR in control
750 or SUGT1-depleted macrophages (**i, k, m, o, q**) or lymphocytes (**j, l, n and p**) that were
751 infected with HIV-1_{ΔEnvNL4-3-Luc} (VSV-G) (**i-p**) or with HIV-1_{ΔEnvNL4-3-IND64E} (VSV-G) (**q**)
752 (n=3).

753 (**r, s**) Representative confocal micrographs of HIV-1_{ICMV-GFP-I-SCEI}-infected HEK293T cells (**r**)
754 and percentages of HIV-1 infected (GFP⁺) cells with γH2AX⁺ foci (**s**) are shown. Means ±
755 SEM are indicated (n=3). P values were calculated using two-tailed unpaired t test (**p
756 <0.01).

757

758 **Figure 3. SUGT1 is associated with microtubules trafficking HIV-1.**

759 (**a**) Representative SIM micrograph of 4 hour HIV-1_{ΔEnvNL4-3-GFP-Vpr} (VSV-G) infected U2OS
760 cells showing SUGT1 and α-tubulin expression (**aI**). (**aII**) is a magnification of the dashed
761 region in (**aI**). (**aIII-4**) are the magnifications of the dashed regions in (**aII**). Fluorescence
762 overlap spectrums of (**aIII-4**) cropped regions, are shown.

763 (**b**) HIV-1 IN and SUGT1 expression levels by WB in control and SUGT1-depleted U2OS
764 cells after 48 hours siRNA transfection and expression of exogenous HIV-1 IN for 24 hours.

765 (c, d) Representative confocal micrographs of HIV-1 HA-IN expression in control and
766 SUGT1-depleted U2OS cells (c) and percentages of cells showing nuclear or diffused HIV-1
767 IN (d).

768 (e) Immunoprecipitation of HA-IN in control and HA-IN-overexpressing HEK293T cells and
769 expression of indicated proteins by WB.

770 WB and images are representative of three independent experiments. Means \pm SEM are
771 indicated from at least three independent experiments. P values were calculated using two-
772 way ANOVA test (**** $p < 0.0001$).

773

774 **Figure 4. SUGT1 stabilizes microtubule tips at the cell cortex.**

775 (a) Representative confocal micrographs and magnifications showing α -tubulin and nucleus
776 in control and SUGT1-depleted U2OS cells.

777 (b) Fluorescence intensity of α -tubulin.

778 (c) Percentages of cells with +MTs parallel or perpendicular to the cell cortex.

779 (d-f) Representative confocal micrographs of α -tubulin, AcK40 α -tubulin and nucleus in
780 control and SUGT1-depleted U2OS cells (d). Magnifications (e). Quantification of AcK40 α -
781 tubulin signals normalized to 100 μ m of cell cortex length in cells (f).

782 (g-i) Representative confocal micrographs of α -tubulin, EB1 and nucleus in control and
783 SUGT1-depleted HeLa cells (g). Separate fluorescence images of (g) are shown in
784 Supplementary Fig. S4g,h. Magnifications (h). Quantification of EB1 comet length (n=559)
785 of cells (n=60) (i).

786 Means \pm SEM are indicated from at least three independent experiments. P values were
787 calculated using two-way ANOVA test for (c) and two-tailed unpaired t test for (f) and (i)
788 (**** $p < 0.0001$).

789

790 **Figure 5. SUGT1 promotes the association between HIV-1 and microtubules.**

791 (a) Co-immunoprecipitation of endogenous SUGT1 with AcK40 α -tubulin in control and
792 HIV-1 $_{\Delta\text{EnvNL4-3-Luc}}$ (VSV-G)-infected U2OS cells for 4 hours and expression of indicated
793 proteins by WB.

794 (b, d) Representative confocal micrographs of HIV-1 $_{\text{IN-EGFP}}$ virus and α -tubulin in control (b)
795 and SUGT1-depleted (d) U2OS cells that were infected for 4 hours.

796 (c) Mander's correlation coefficient (tM1) of HIV-1 $_{\text{IN-EGFP}^+}$ and α -tubulin in control and
797 SUGT1-depleted U2OS cells at 4 h.p.i..

798 (e) Percentages of cells showing nuclear or cytoplasmic HIV-1 $_{\text{IN-EGFP}^+}$ events at 4 and 6 h.p.i..

799 (f) Representative confocal micrographs of HIV-1 $_{\text{IN-EGFP}}$, $\square\square\square$ and nucleus in control and
800 SUGT1-depleted HeLa cells that were infected with HIV-1 $_{\text{IN-EGFP}}$ for 6 hours. Magnifications
801 are shown.

802 (g) Lengths of EB1 comets (n=400) of cells (n=100) are determined.

803 (h) Percentages of control or SUGT1-depleted HeLa cells showing nuclear or only
804 cytoplasmic HIV-1 $_{\text{IN-EGFP}^+}$ events at 6 h.p.i.

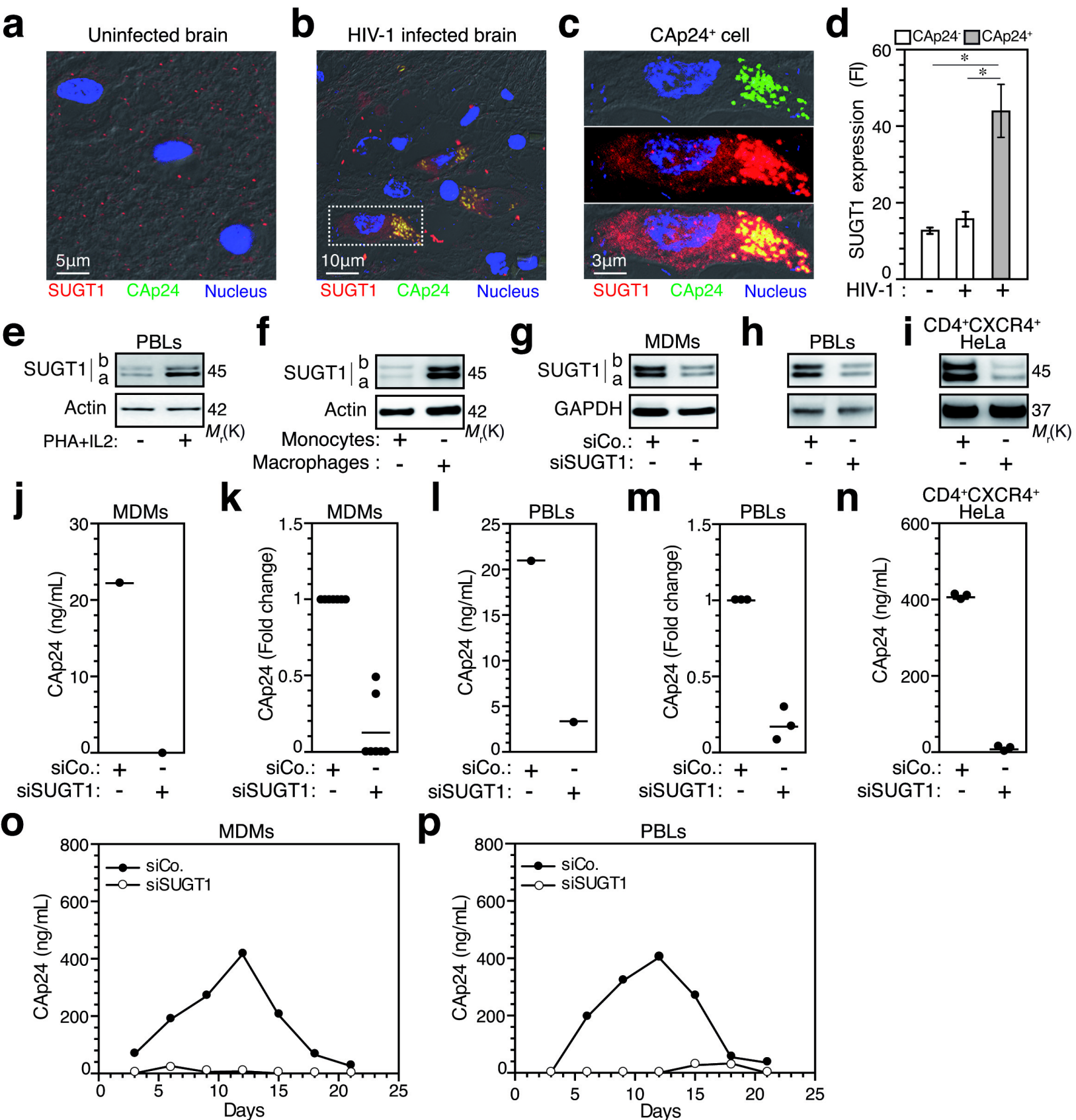
805 Means \pm SEM are indicated from at least three independent experiments. P values were
806 calculated using two-tailed unpaired t-test for (c) and (g) and two-Way ANOVA for (e) and
807 (h) (**p<0.001 and ****p<0.0001).

808

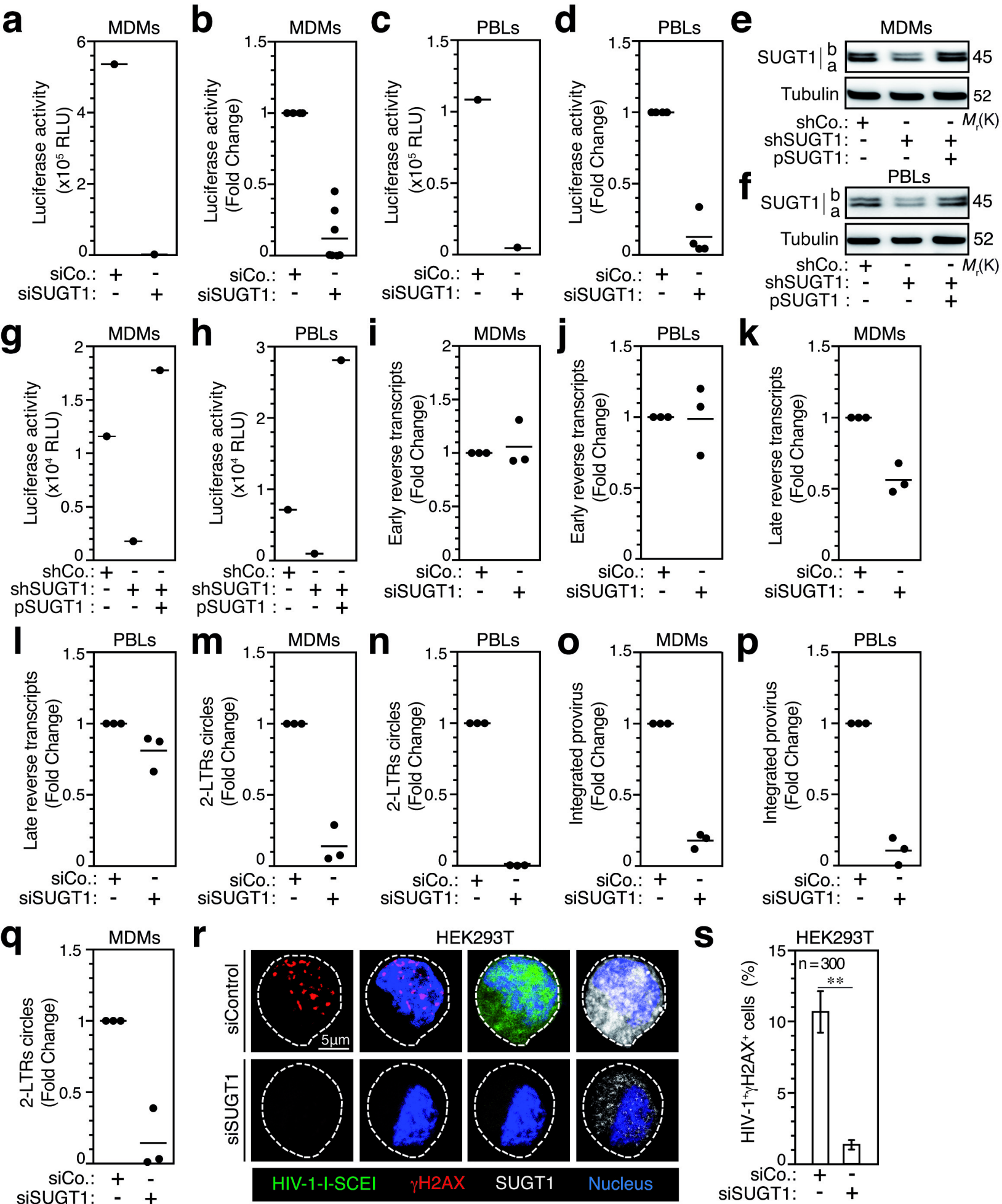
809 **Figure 6. SUGT1 depletion impairs replication of HIV-1 primary isolates and ART**
810 **mutant resistant virus.**

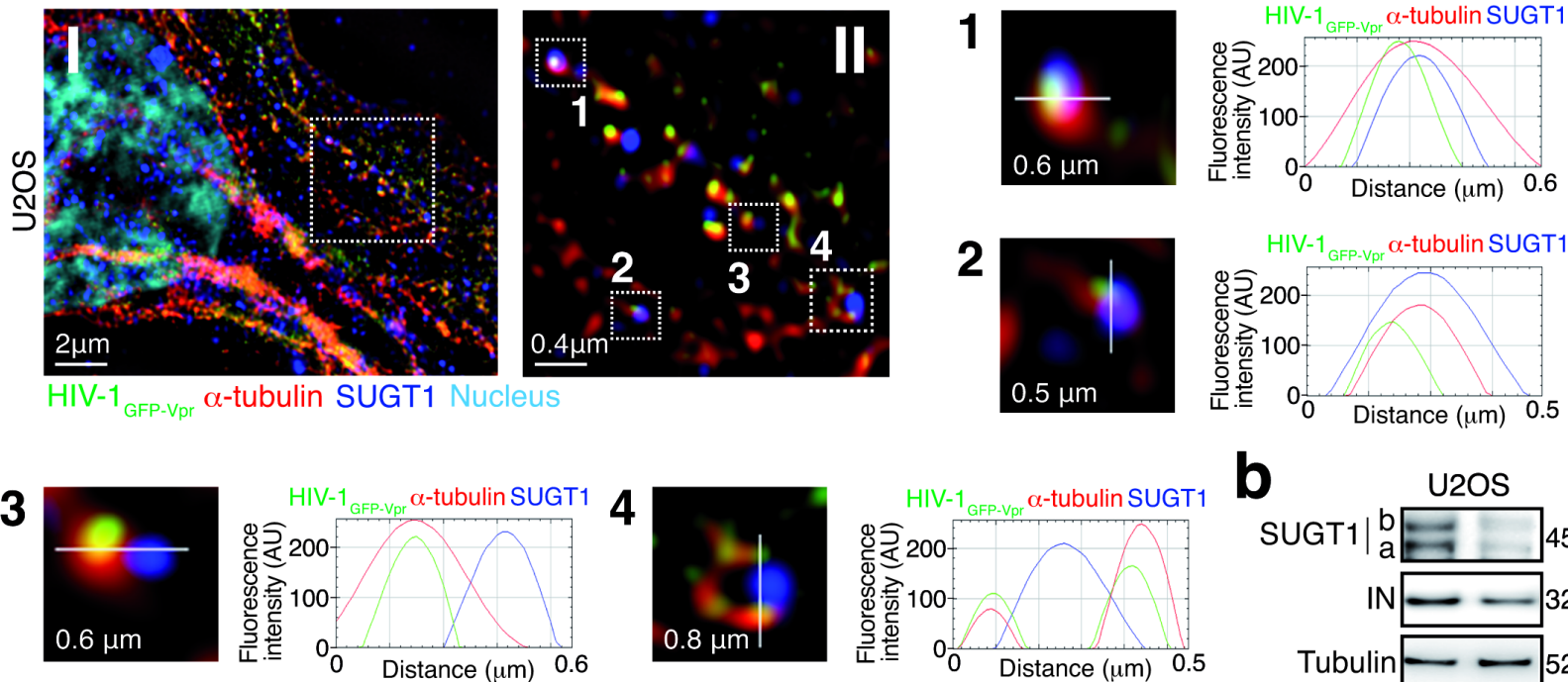
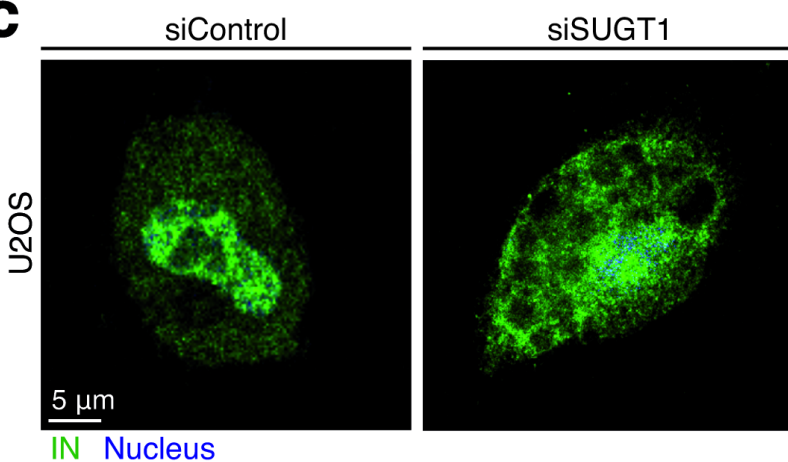
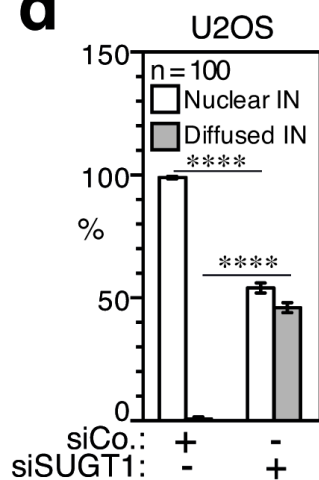
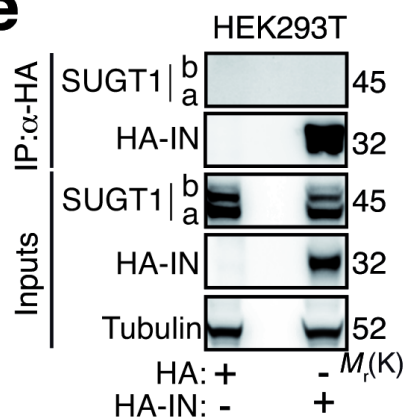
811 (a-d) HIV-1 2-LTRs circles quantification by qPCR 72 h.p.i. with HIV-1 $_{\text{BX08}}$ (a, b) and HIV-
812 $1_{132\text{W}}$ (c, d) primary isolates of control and MDMs that were silenced for SUGT1 during 72
813 hours. Representative donor (a, c) and fold changes (n=3) (b, d) are shown.

814 **(e-g)** HIV-1 C_{Ap}24 detected by WB in the cell supernatants (SN) of MDMs that were
815 depleted (or not) for SUGT1 and infected with HIV-1_{BXO8} **(e)**, HIV-1_{132W} **(f)** and HIV-1_{DH12}
816 **(g)**. Representative WB revealing C_{Ap}24, SUGT1 and Tubulin expressions are shown (n=3).
817 **(h, i)** Control and SUGT1-depleted primary human MDMs were infected with HIV-1_{140/148}
818 and evaluated for proviral integration and for C_{Ap}24 release at 72 h.p.i. (n=2).
819

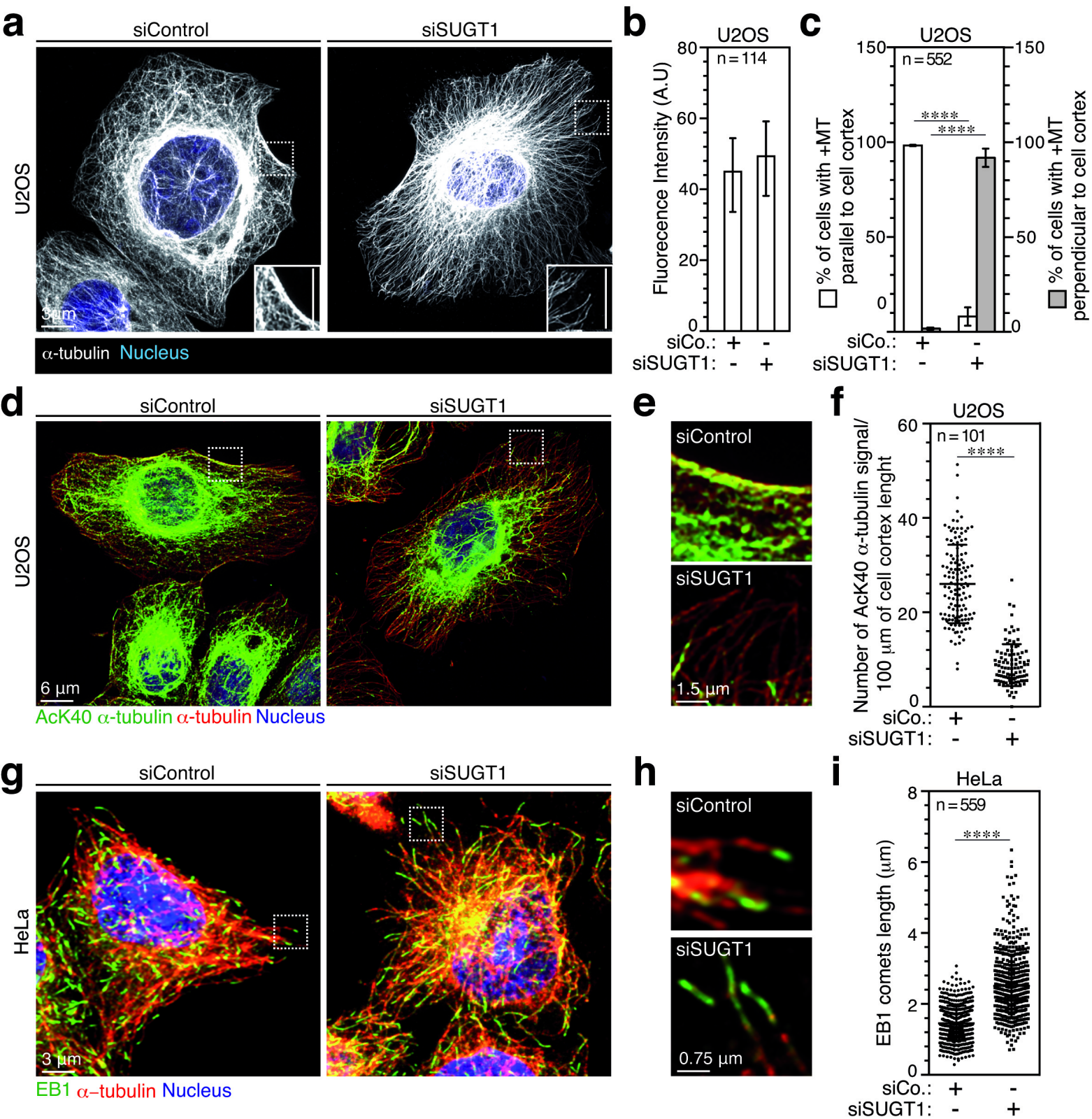


ALLOUCH CDD Revised#1

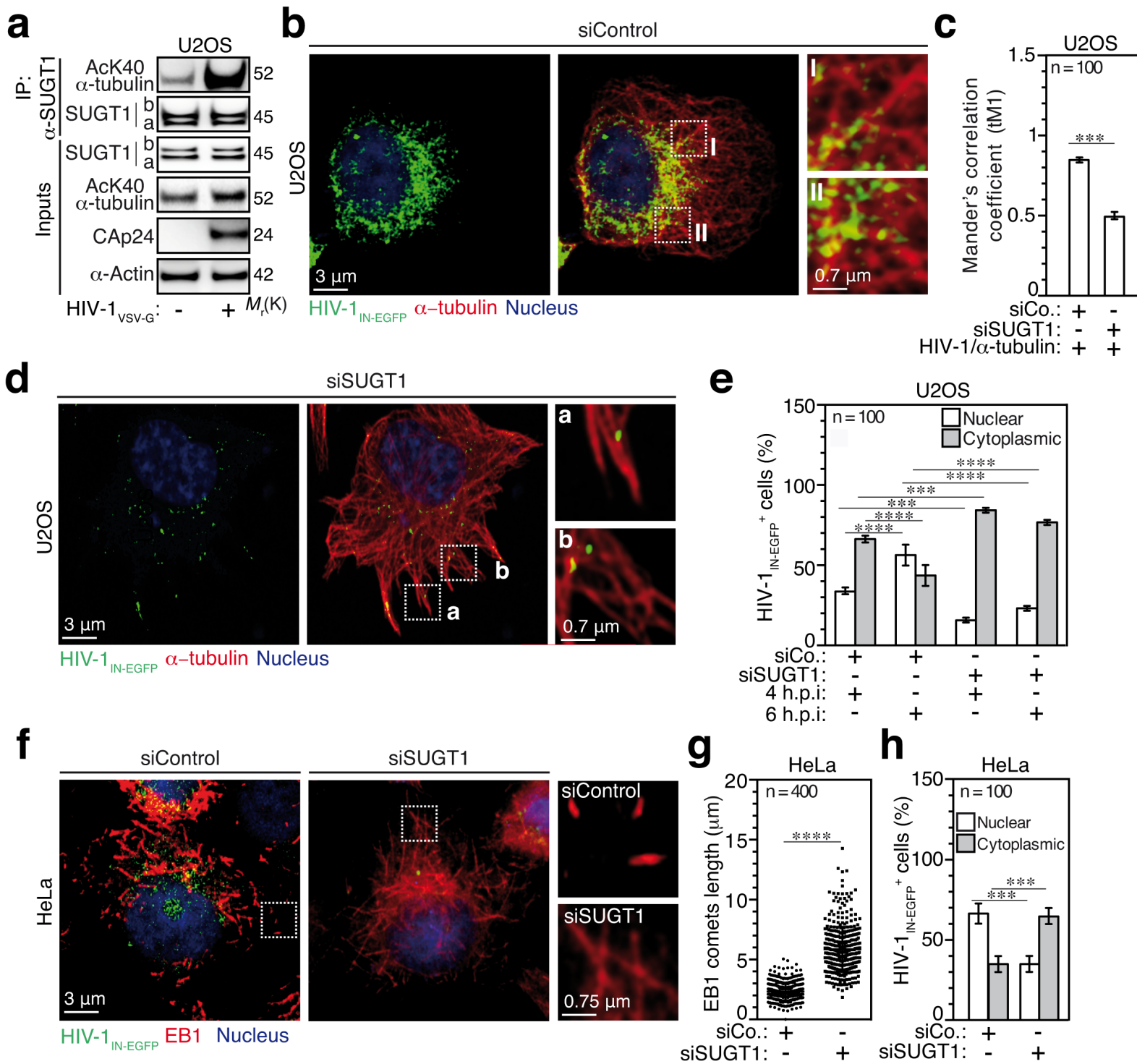


a**b****c****d****e**

ALLOUCH CDD Corrected#3



ALLOUCH CDD Revised#4



ALLOUCH CDD Corrected#5

